ChemComm

COMMUNICATION

View Article Online
View Journal

Cite this: DOI: 10.1039/d6cc02124g

Received 7th April 2026,
Accepted 21st May 2026

DOI: 10.1039/d6cc02124g

rsc.li/chemcomm

Direct solvothermal crystallisation of the metastable cubic perovskite $CsMnF_3$ and its magnetism

Craig I. Hiley, [a] Catriona A. Crawford, [a] Clemens Ritter, [b] Mark S. Senn *[a] and Richard I. Walton *[a]

The solvothermal synthesis of polycrystalline cubic $CsMnF_3$ at 100 °C is reported, a phase previously prepared phase-pure only at 700 °C and 30 kbar. *In situ* powder X-ray diffraction, shows that cubic $CsMnF_3$ transforms irreversibly to the 6H polymorph at ~500 °C. The magnetic properties of cubic $CsMnF_3$ are characterised by G-type antiferromagnetic ordering, as determined from powder neutron diffraction.

The solvothermal synthesis of a wide variety of oxide perovskites has been documented in the literature; this includes various ABO_3 compositions that would usually be expected to crystallise using the high temperatures associated with solid-state chemistry, such as ferroelectric titanates, and niobates, multiferroic chromites and ferrates, magnetoresistive manganites, and superconducting bismuthates.[1] The advantage of direct crystallisation from solution, often under hydrothermal conditions when water is used, is access to materials with small crystallite size (micron to nanometre dimensions) that may be annealed into fine-grained electroceramics, or used in sensing or heterogeneous catalysis because of their high surface areas.[2–4] The synthesis of oxides from solution can also allow access to unexpected polymorphs, either metastable crystal forms that subsequently collapse on further heating, such as the ilmenite structure of $NaNbO_3$,[5] or structures usually only stable at higher temperatures, such as the cubic polymorph of $BaTiO_3$.[6]

Fluoride perovskites have been less studied than their oxide analogues, which may be due to the corrosive nature of many fluoride precursors (fluorine gas or HF, for example) that makes routine synthesis challenging.[7] Solvothermal routes to metal fluorides offer an attractive way for their convenient preparation, with the use of closed reaction vessels and solution precursors that are easy to handle. Examples include Na_2FeF_4[8] and $NaMF_3$ (M = Mn, Fe, Co, Ni),[9] and oxyfluorides, not accessible by other routes, such as the M(OH)F diaspores.[10,11] Herein we study the solvothermal crystallisation of $CsMnF_3$ and reveal an example of a polymorph-selective synthesis, where a crystal form previously reported at high temperature and pressure[12] is formed directly under mild conditions.

An initial sample of $CsMnF_3$ synthesised by the solvothermal reaction between the binary fluorides CsF and MnF_2 in ethylene glycol at 160 °C was found to contain mostly the cubic polymorph of $CsMnF_3$ and some unreacted MnF_2, ~20 wt% of the sample as determined by phase quantification from Rietveld fitting against laboratory XRD (Fig. S1a). Increasing the synthesis temperature to 180 °C increased the amount of MnF_2 remaining in the sample, whilst lowering the synthesis temperature revealed a near-linear relationship between temperature and MnF_2 content (Fig. S1b), with no significant effect on the crystallinity of the cubic $CsMnF_3$ phase. Rietveld analysis of the laboratory XRD from a sample prepared at 100 °C suggested that <2.5 wt% MnF_2 is present in this sample. This sample was used in further characterisation experiments (except neutron powder diffraction, see Experimental and below).

Synchrotron powder XRD was collected using beamline I11,[13] (Diamond Light Source, UK) from the sample synthesised at 100 °C. Rietveld analysis of the diffraction data from the sample at room temperature suggested the sample contained 2.4(1) wt% MnF_2, and revealed an additional small (1.3(1) wt%) impurity of 6H-$CsMnF_3$ which was not detected by laboratory XRD. The remainder (96.3(1) wt%) was cubic $CsMnF_3$ and these three phases account for all observed diffraction peaks (Fig. 1a). Upon cooling to 100 K, the main phase remains cubic with a contraction of the lattice parameter a (Fig. 1c inset). A quartz capillary filled with a specimen from the same sample had slightly higher refined weight fractions of MnF_2 and 6H-$CsMnF_3$ at room temperature (6.63(7) wt% and 2.93(3) wt%, respectively). Upon heating, no significant changes are observed up to 300 °C.

[a] Department of Chemistry, University of Warwick, Gibbet Hill Road, Coventry, CV4 7AL, UK. E-mail: r.i.walton@warwick.ac.uk, m.senn@warwick.ac.uk
[b] Institut Laue-Langevin, 71 Avenue des Martyrs, CS20156, 38042 Grenoble Cédex 9, France

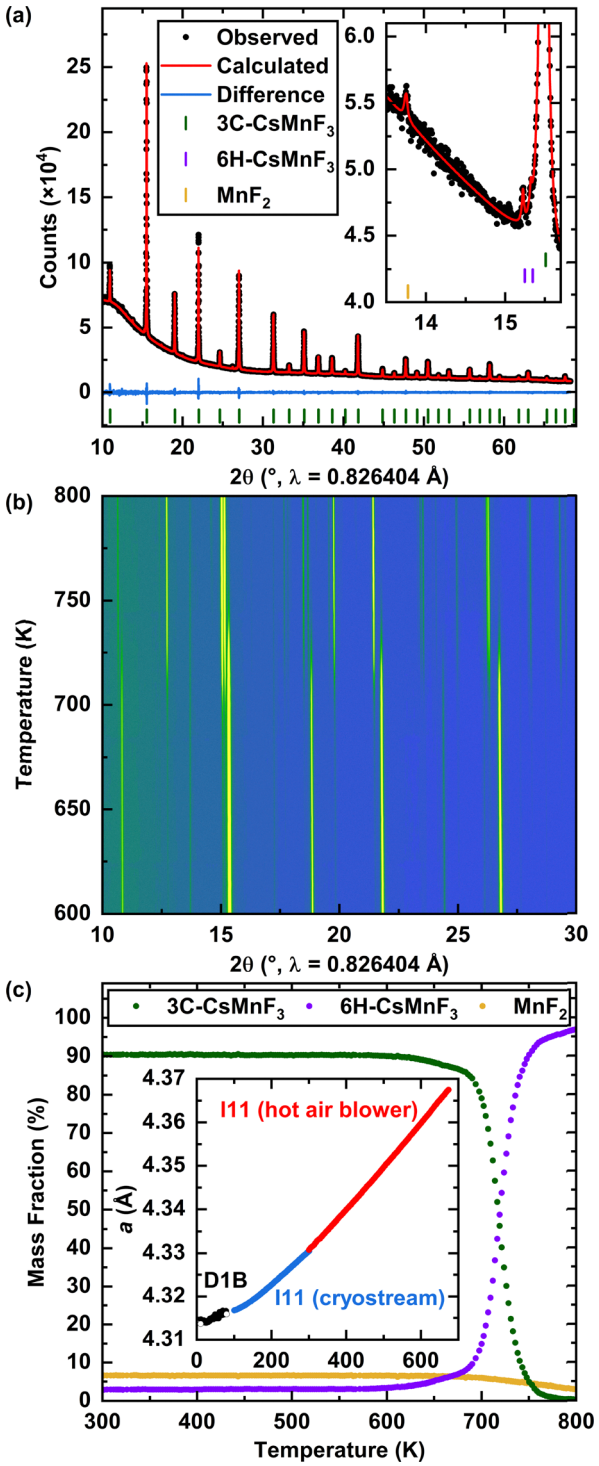

Fig. 1 (a) Three-phase Rietveld fit to synchrotron XRD collected from a sample of cubic (3C) $CsMnF_3$ at 300 K (in borosilicate capillary). Tick marks for 6H-$CsMnF_3$ and MnF_2 impurities omitted for clarity. Inset shows weak peaks from impurity phases (with tick marks shown). (b) Synchrotron X-ray diffraction contour plot measured as a function of temperature, shown over phase transition temperature region. (c) Refined mass fractions of crystalline phases from sample (in quartz capillary) using synchrotron XRD upon heating. Inset shows refined lattice parameter, *a*, as a function of temperature measured using three diffraction experiments. For D1B, open and closed symbols were measured using a short (1.28 Å) and long (2.52 Å) neutron wavelengths, respectively.

Above 300 °C, a phase transition from cubic $CsMnF_3$ to 6H-$CsMnF_3$ occurs, which is complete by 500 °C (773 K, Fig. 1b and c). This shows that the cubic polymorph is metastable and it is unlikely that it can be synthesised by a conventional solid-state reaction at ambient pressure. Additionally, the amount of MnF_2 gradually decreases from ~400 °C, with additional, unidentified peaks appearing from 450 °C, which is likely to be caused by reaction with air in the capillary or with the quartz capillary (Fig. S2).

The Goldschmidt tolerance factor, *t*, of $CsMnF_3$ is 1.06 is close to a cubic–hexagonal threshold, so it is not obvious from *t* alone which polymorph is likely to form. Previous high temperature syntheses of the hexagonal polymorph, and the phase transition observed here from cubic to 6H-$CsMnF_3$ upon heating, suggest that latter is the most thermodynamically stable polymorph. However, the isolation of the cubic polymorph from low temperature solution syntheses may suggest that the formation of face-sharing MnF_6 octahedral environments has a significantly higher activation energy, likely due to the shorter cation-cation distances and hence repulsion.[14]

The magnetic susceptibility of cubic $CsMnF_3$ shows variation as a function of temperature that is indicative of antiferromagnetic order, with a Néel temperature (T_N) of approximately 70 K (Fig. 2a). This is in contrast to 6H-$CsMnF_3$, which has a complex magnetic structure with antiferromagnetic and ferrimagnetic exchange pathways that has not been fully resolved.[15–17] A linear fit to the high temperature, paramagnetic region (350 K $\leq T \leq$ 400 K) of the inverse molar susceptibility gives a good agreement and can be interpreted by the Curie–Weiss law (Fig. 2a). This gives a Curie–Weiss temperature, θ_{CW}, of −94.5(8) K, which indicates net antiferromagnetic interactions and an effective moment per Mn^{2+} ion, μ_{eff}, of 6.29(2)μ_B. High spin Mn^{2+} has no orbital angular momentum ($L = 0$) and its spin-only moment is 5.92μ_B. A 6.3 wt% MnF_2 impurity is sufficient to account for the discrepancy between μ_{eff} and the spin-only value, which is concordant with the mass fraction obtained by Rietveld refinement against powder synchrotron XRD from the sample in a quartz capillary (refined to 6.63(7) wt%). The literature shows that the μ_{eff} of octahedral high spin Mn^{2+} (and Fe^{3+}, another ^6S ion) has been reported to be between 6.1μ_B and 6.4μ_B in several other fluorides, oxides and phosphates.[15,18–26] This divergence has sometimes been attributed to short range correlation persisting above T_N, or slight deviation from an ideal octahedral environment. These effects are unlikely to be the cause of a larger-than-expected μ_{eff} in cubic $CsMnF_3$; it has a regular octahedral environment for Mn (on average) and the Curie–Weiss fit was carried out across a temperature range of 350 – 400 K, much greater than T_N (~70 K).

Variable temperature neutron powder diffraction data[27] were collected using the D1B[28] powder diffractometer (Institut Laue-Langevin, France). To prepare the large powder sample (~5 g) for neutron diffraction, a synthesis scaled up by a factor of 10 was employed (see Experimental). This sample was found to contain an increased amount of MnF_2 (18.2 wt%, by Rietveld analysis of neutron powder diffraction) compared to the

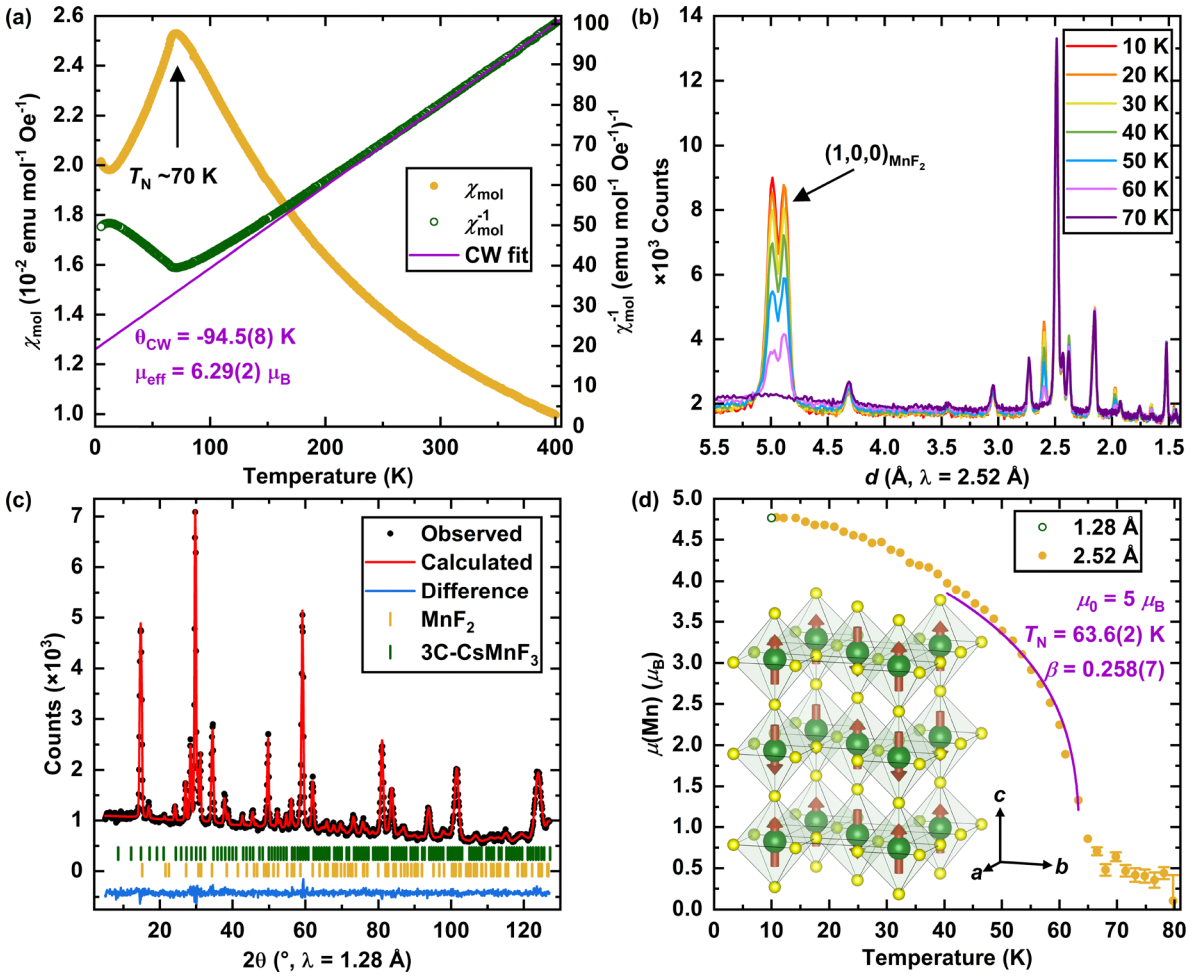

Fig. 2 (a) Molar magnetic susceptibility of cubic $CsMnF_3$ as a function of temperature in an applied field of 1000 Oe, with a Curie–Weiss (CW) fit to the inverse molar magnetic susceptibility. (b) Variable temperature neutron diffraction in 10 K increments, plotted in *d*-space. (c) Two-phase (cubic $CsMnF_3$ and MnF_2) magnetic Rietveld fit to neutron powder diffraction data at 10 K. Tick marks for both phases include magnetic superstructure peaks (d) Refined Mn^{2+} moment in cubic $CsMnF_3$ as a function of temperature with a fit using a critical power law (see text). Inset shows the G-type antiferromagnetic ordering in cubic $CsMnF_3$ structure, with Cs ions omitted for clarity. *n.b.* All neutron powder diffraction data presented in (b)–(d) were measured from a different sample containing ~18 wt% MnF_2.

original sample. When cooled below T_N, $CsMnF_3$ remains apparently cubic, though several magnetic superstructure peaks develop in the neutron diffraction pattern at d = 4.98 Å, 2.06 Å, 1.98 Å and 1.67 Å, as well as the main antiferromagnetic superstructure[29] peak (100) from MnF_2 at d = 4.87 Å (partly overlapping with a cubic $CsMnF_3$ peak, Fig. 2b), which has a similar T_N. A fit to the neutron diffraction pattern at 10 K (Fig. 2c) shows cubic $CsMnF_3$ has G-type antiferromagnetic ordering at 10 K, with a moment of 4.77(2) μ_B (Fig. 2d, inset). The moment direction could not be uniquely determined from the powder data. This model was used to fit to the variable temperature data upon heating to 80 K, with lattice parameter a slightly increasing (Fig. 1c, inset) and the Mn magnetic moment, μ(Mn), undergoing an exponential decay (Fig. 2d). Close to the T_N (40 K < T < 65 K), μ(Mn) can be fitted using a critical power law, with the saturated moment, μ_0, fixed at the 2S value of 5μ_B. The fit yields a T_N of 63.6(2) K and a critical exponent, β, of 0.258(7), suggesting a significant deviation from a mean field system (β = 0.5) or simple 3D Heisenberg or Ising antiferromagnetic systems (β = 0.365 and 0.325, respectively).[30] A β close to 0.25 may suggest a tricritical point.[31]

Fig. 3 compares the crystal structures of the two polymorphs studied here, showing the different connectivity of the Mn-centred octahedra. The application of pressure to hexagonal perovskites has been found to destabilise the B cations in face-sharing octahedra due to B-B repulsion.[32,33] In particular, Kafalas and Longo[12] found the $CsBF_3$ (B = Mg, Mn–Ni, Zn) hexagonal perovskites convert to hexagonal polytypes with an increasing proportion of *ccp* layers with application of pressure, with a transition from the 6H to the cubic ("3C") polymorph seen in $CsMnF_3$ and $CsFeF_3$ when quenched from 700 °C at 30 and 80 kbar, respectively, whose tolerance factors (1.06 and 1.07 respectively) are closest to the cubic–hexagonal threshold.

A synthesis of an impure sample cubic nanocrystalline $CsMnF_3$ was recently reported by Fellner and Lauria[34] from Mn(II) acetate and CsF (1 : 3 ratio, respectively) in a mixture of

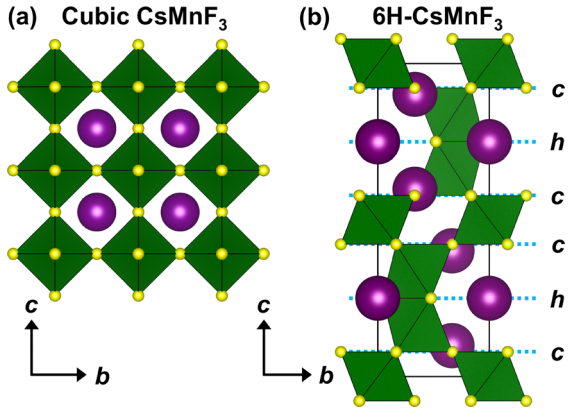

Fig. 3 (a) Cubic and (b) 6H-$CsMnF_3$ with purple Cs cations purple, green MnF_6 octahedra and yellow F anions. In (b), the packing of the CsF_3 layers are denoted either *c* or *h* to denote cubic or hexagonal close packing, respectively.

oleic acid and octadecene at 160 °C. This sample was contaminated with a significant amount of an acid fluoride phase $Cs_2H_3F_5$ (though the diffraction pattern of $Cs_2H_3F_5$ has been indexed to a face-centred cubic cell, its crystal structure has not previously been determined, making quantitative analysis impossible). The AC magnetic susceptibility as a function of temperature of the mixed $CsMnF_3$-$Cs_2H_3F_5$ sample suggested antiferromagnetic ordering occurred at a low temperature (<60 K, though this can be affected by the oscillating field frequency in AC susceptibility measurements[35]). Scanning electron microscopy (SEM) from the sample prepared by our synthesis route shows crystallites with a predominant rod-like morphology (Fig. 4a) with dimensions of ~0.1 μm × ~0.4 μm, contrasting with the 5 nm crystallites observed in the sample reported by Fellner and Lauria.[34] When the sample was heated to 748 K (475 °C) under N_2 for 1 hr, 6H-$CsMnF_3$ is produced with crystallites that generally retain the rod-like morphology though an increase in crystallite size (Fig. 4b).

In summary, we have prepared high purity cubic $CsMnF_3$ by a solvothermal reaction in ethylene glycol that allows its phase transitions and magnetic behaviour to be studied in detail. We have shown that it converts to the thermodynamic 6H polymorph upon heating to ~450 °C, demonstrating its metastability. Cubic $CsMnF_3$ is a G-type antiferromagnet with T_N ~ 70 K.

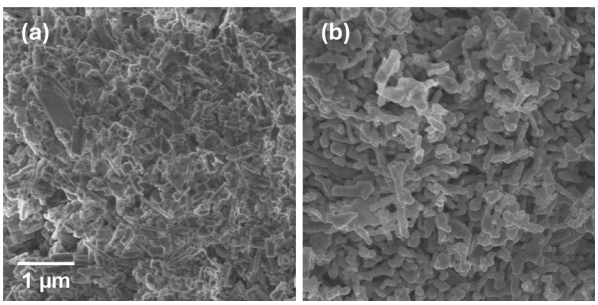

Fig. 4 SEM images of (a) as-made cubic $CsMnF_3$ and (b) 6H-$CsMnF_3$ made by heating of the cubic polymorph. Scale bar the same for both.

The preparative chemistry developed could be applicable to other transition-metal fluorides with the prospect of discovery of novel compositions and crystal structures.

Conflicts of interest

The authors declare that they have no known competing financial interests or personal relationships that could have appeared to influence the work reported in this paper.

Data availability

All data generated or analysed during this study are included in this article and the supplementary information (SI). Supplementary information is available. See DOI: https://doi.org/10.1039/d6cc02124g.

Data from ILL available at https://dx.doi.org/10.5291/ILL-DATA.5-24-770.

Acknowledgements

R. I. W. and M. S. S. acknowledge the Leverhulme Trust for a research project grant (Grant No. RPG-2022-22). M. S. S. acknowledges the Royal Society for a fellowship (UF160265 and URF\R\231012). Initial sample characterisation was performed *via* the Warwick X-ray and Microscopy Research Technology Platforms. We thank Professor Martin R. Lees for access to SQUID magnetometer. Synchrotron powder XRD was supported by the Diamond Light Source Oxford-Warwick BAG CY39378-4, and the Institut Laue-Langevin provided neutron diffraction under experiment 5-24-770 (DOI: https://doi.org/10.5291/ILL-DATA.5-24-770). We thank Putthachat Sinted for assistance with neutron diffraction measurement and Andrew Unsworth for electron microscopy support.

References

1 R. I. Walton, *Chem. – Eur. J.*, 2020, **26**, 9041–9069.
2 J. Zhu, H. Li, L. Zhong, P. Xiao, X. Xu, X. Yang, Z. Zhao and J. Li, *ACS Catal.*, 2014, **4**, 2917–2940.
3 C. Si, W. Zhang, Q. Lu, E. Guo, Z. Yang, J. Chen, X. He and J. Luo, *Catalysts*, 2022, **12**, 601.
4 X. Xue and B. Li, *Nanomaterials*, 2025, **15**, 472.
5 D. R. Modeshia, R. J. Darton, S. E. Ashbrook and R. I. Walton, *Chem. Commun.*, 2009, 68–70.
6 I. J. Clark, T. Takeuchi, N. Ohtori and D. C. Sinclair, *J. Mater. Chem.*, 1999, **9**, 83–91.
7 A. Tressaud, *J. Fluorine Chem.*, 2025, **281**, 110374.
8 Q. Yan, H. Xu, K. Hoang, X. Zhou, P. Kidkhunthod, P. Lightfoot, W. Yao and Y. Tang, *Appl. Phys. Lett.*, 2022, 121.
9 C. A. Crawford, C. I. Hiley, J. Gainza, C. Ritter, R. I. Walton and M. S. Senn, *Phys. Rev. B*, 2025, **112**, 035150.
10 C. A. Crawford, C. I. Hiley, C. A. M. Scott, C. Ritter, M. R. Lees, N. C. Bristowe, R. I. Walton and M. S. Senn, *Inorg. Chem.*, 2024, **63**, 9184–9194.
11 H. Ben Yahia, M. Shikano, M. Tabuchi, H. Kobayashi, M. Avdeev, T. T. Tan, S. Liu and C. D. Ling, *Inorg. Chem.*, 2014, **53**, 365–374.
12 J. M. Longo and J. A. Kafalas, *J. Solid State Chem.*, 1969, **1**, 103–108.
13 S. P. Thompson, J. E. Parker, J. Potter, T. P. Hill, A. Birt, T. M. Cobb, F. Yuan and C. C. Tang, *Rev. Sci. Instrum.*, 2009, 80.
14 R. H. Mitchell, *Perovskites: Modern and Ancient*, Almaz Press, 2002.

15 X. Zhu, Y. Zhao, S. Zhang, J. Wu, D. Shao, E. Song, Q. Zhang, C. Yin and S. Ye, *J. Phys. Chem. C*, 2021, **125**, 27800–27809.
16 Y. Yamaguchi and T. Sakuraba, *J. Phys. Soc. Jpn.*, 1975, **38**, 1011–1019.
17 A. Oleaga, A. Salazar and Y. M. Bunkov, *J. Phys.: Condens. Matter*, 2014, **26**, 096001.
18 T. Li, R. Clulow, A. J. Bradford, S. L. Lee, A. M. Z. Slawin and P. Lightfoot, *Dalton Trans.*, 2019, **48**, 4784–4787.
19 T. Li, A. J. Bradford, S. L. Lee and P. Lightfoot, *Chem. Mater.*, 2024, **36**, 5228–5237.
20 A. Winterstein, H. Akamatsu, D. Möncke, K. Tanaka, M. A. Schmidt and L. Wondraczek, *Opt. Mater. Express*, 2013, **3**, 184–193.
21 M. B. Sanders, J. W. Krizan, K. W. Plumb, T. M. McQueen and R. J. Cava, *J. Phys.: Condens. Matter*, 2017, **29**, 045801.
22 A. A. Zatsiupa, L. A. Bashkirov, I. O. Troyanchuk, G. S. Petrov, A. I. Galyas, L. S. Lobanovskii, S. V. Trukhanov and I. M. Sirota, *Inorg. Mater.*, 2013, **49**, 616–620.
23 K. Matan, B. M. Bartlett, J. S. Helton, V. Sikolenko, S. Mat'aš, K. Prokeš, Y. Chen, J. W. Lynn, D. Grohol and T. J. Sato, *et al.*, *Phys. Rev. B*, 2011, **83**, 214406.
24 E. Solana-Madruga, A. J. Dos santos-García, A. M. Arévalo-López, D. Ávila-Brande, C. Ritter, J. P. Attfield and R. Sáez-Puche, *Dalton Trans.*, 2015, **44**, 20441–20448.
25 X. Zhu, S. Meng, Y. Zhao, S. Zhang, J. Zhang, C. Yin and S. Ye, *J. Phys. Chem. Lett.*, 2020, **11**, 9587–9595.
26 H. Ueda, T. Inamori, A. Taguchi, C. Michioka and K. Yoshimura, *J. Phys. Soc. Jpn.*, 2021, **91**, 014704.
27 P. Sinted, C. A. Crawford, C. I. Hiley, V. Nassif, C. Ritter, M. S. Senn and R. I. Walton, *Investigation of Phase Transitions of Mixed A-site Perovskites* $K_{1-x}Rb_xMnF_3$ ($x \leq 1$), Institut Laue-Langevin, 2025, DOI: 10.5291/ILL-DATA.5-24-770.
28 I. P. Orench, J. F. Clergeau, S. Martínez, M. Olmos, O. Fabelo and J. Campo, *J. Phys.: Conf. Ser.*, 2014, **549**, 012003.
29 Z. Yamani, Z. Tun and D. H. Ryan, *Can. J. Phys.*, 2010, **88**, 771–797.
30 H. E. Stanley, *Introduction to phase transitions and critical phenomena*, University Press, Oxford, 1987.
31 N. E. Massa, L. del Campo, D. de Souza Meneses, P. Echegut, G. F. L. Fabbris, G. D. M. Azevedo, M. J. Martínez-Lope and J. A. Alonso, *J. Appl. Phys.*, 2010, 108.
32 K. Oka, M. Azuma, S. Hirai, A. A. Belik, H. Kojitani, M. Akaogi, M. Takano and Y. Shimakawa, *Inorg. Chem.*, 2009, **48**, 2285–2288.
33 Y. Li, J. Cheng, J. A. Alonso, J. B. Goodenough and J. Zhou, *Inorg. Chem.*, 2017, **56**, 8187–8194.
34 M. Fellner and A. J. Lauria, *Sol-Gel Sci. Technol.*, 2023, **107**, 259–268.
35 C. V. Topping and S. J. Blundell, *J. Phys.: Condens. Matter*, 2019, **31**, 013001.